JACS
JOURNAL OF THE AMERICAN CHEMICAL SOCIETY
Article
pubs.acs.org/JACS

# Growth Mechanism of Microporous Zincophosphate Sodalite Revealed by In Situ Atomic Force Microscopy

Mark A. Holden, Pablo Cubillas, Martin P. Attfield, James T. Gebbie, and Michael W. Anderson*

Centre for Nanoporous Materials, School of Chemistry, The University of Manchester, Oxford Road, Manchester M13 9PL, United Kingdom

Supporting Information

**ABSTRACT:** Microporous zincophosphate sodalite crystal growth has been studied in situ by atomic force microscopy. This simple model system permits an in depth investigation of some of the axioms governing crystal growth of nanoporous framework solids in general. In particular, this work reveals the importance of considering the growth of a framework material as the growth of a dense phase material where the framework structure, nonframework cations, and hydrogen-bonded water must all be considered. The roles of the different components of the structure, including the role of strict framework ordering, are disentangled, and all of the growth features, both crystal habit and nanoscopic surface structure, are explained according to a simple set of rules. The work describes, for the first time, both ideal growth and growth leading to defect structures on all of the principal facets of the sodalite structure. Also, the discovery of the presence of anisotropic friction on a framework material is described.

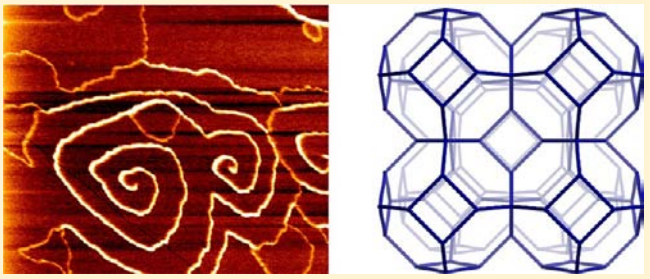

## 1. INTRODUCTION

Understanding how microporous crystals grow is important for control at the nanoscale. This is necessary to influence crystal habit and size, concentration and type of defects, intergrowth switching, and the use, or not, of expensive organic templating agents. In this regard, we have engaged in an extensive program of study to use atomic force microscopy (AFM)[1−26] and other state-of-the-art techniques, to probe in situ the nanoscopic mechanisms of crystal growth of this important class of materials. The choice of system to study to garner the most information is important and depends upon a number of factors, some of which relate to the importance of the framework type and some to the nature of the AFM probe. To interrogate crystal growth by in situ AFM, whereby the growth is monitored in real time, the zincophosphate zeolite analogues are particularly profitable. This relates in large part to the fact that they can usually be grown from solution close to room temperature, from clear solutions, and at growth rates readily amenable to AFM observation.[23,24] In this work, we have chosen to study the crystal growth of zincophoshphate sodalite (ZnPO-SOD). The reason for the choice of framework structure SOD is at least 3-fold: first, the framework structure is built up entirely from one cage type making it, in principle, one of the simplest structural systems in this class. Second, the strict alternation of zinc and phosphorus in the framework mimics the strict alternation of aluminum and silicon in highly aluminous zeolites. This in turn imparts strict rules on cation location in extra-framework sites. Third, the SOD structure can be replicated in a wide variety of chemical compositions from silicates to metal−organic frameworks (MOFs), and this work fits into a larger study across the breadth of these materials.

Sodalite, $Na_6Al_6Si_6O_{24}(NaCl)_2$, is an abundant mineral with a structure originally determined by Pauling.[27] Natural and synthetic versions can accommodate a large variety of compositional variation, with framework atom substitutions including Be, Ga, Ge, P, Zn, and As.[28−31] The sodalite framework is comprised of truncated octahedral cages known as sodalite cages that are fused together through 4-ring or 6-ring channels to create the framework.[27] This material has been of interest due to potential applications in a range of processes, such as storage of hydrogen,[32] storage of the nuclear waste product $^{85}Kr$,[33,34] photochromism,[35] and removal of water/small molecules in industry.[36,37] The study of sodalite is also important, because the sodalite cage, or $\beta$-cage, is a common structural unit in a variety of other frameworks, such as LTA, EMT, and FAU.[38]

In 1991, the first report of a new class of zeotype, the zincophosphates, was published by Nenoff et al.[39] These materials could be synthesized at conditions from room temperature upward, and included both known frameworks, such as SOD, FAU, and *Li*A(BW),[29] as well as new framework types such as the chiral CZP framework.[40,41] Because the syntheses of these materials could be performed at room temperature, they are particularly amenable for study by AFM. In our previous communication, the first in situ AFM measurements of a zeotype were performed on sodalite

**Received:** May 1, 2012
**Published:** July 6, 2012





dx.doi.org/10.1021/ja303814p | J. Am. Chem. Soc. 2012, 134, 13066−13073

zincophosphate.[23] These studies revealed an interlacing spiral growth mechanism on the {100} facets of the crystals caused by anisotropic growth rates resulting from the alternation of zinc and phosphorus in the structure. In this work, a much more detailed study of the growth of this structure has been conducted establishing the growth mechanism on all principal crystal facets as well as the consequences of defect incorporation.

## 2. EXPERIMENTAL SECTION

AFM measurements were made using a JPK Instruments AG NanoWizard II operating in contact mode. Ex situ scans were obtained at a scan rate of 2 Hz, while in situ scans were obtained at 4 Hz. $Si_3N_4$ cantilevers were used with a nominal force constant of 0.58 N $m^{-1}$ (Veeco model NP-10). In situ experiments were performed by first attaching a seed crystal to a glass slide using an epoxy resin cured at 60 °C, followed by addition of a growth solution.

Seed crystals were synthesized following the room temperature method of Gier and Stucky;[29] however, the seed crystal synthesis was performed at 4 °C. The growth solutions for in situ experiments were prepared in two ways. In the first case, the mother liquor was extracted toward the end of a typical synthesis following the recipe of Gier and Stucky (ca. 6 h), then added to the crystals before scanning commenced. In the second case, solutions were prepared in the laboratory replicating Zn/P/Na concentrations found in the mother liquor. Typical laboratory solutions were prepared with composition of 4−30 ppm zinc ($Zn(NO_3)_2$), 3000 ppm phosphorus ($H_3PO_4$), 20 000 ppm sodium (NaBr), and adjusted to pH 7 using NaOH. Because zinc was the limiting ion, this concentration was varied to alter the supersaturation.

## 3. RESULTS AND DISCUSSION

Figure 1a shows the typical morphology of the seed crystals used throughout this study. ZnPO-SOD belongs to space group

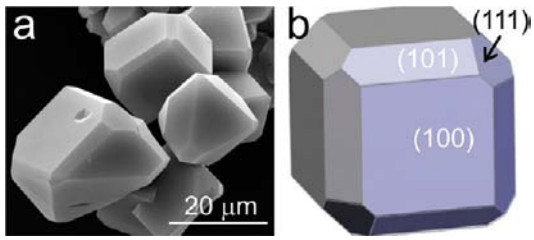


**Figure 1.** (a) SEM micrograph showing the typical morphologies of ZnPO-SOD crystals, and (b) schematic diagram showing allowed habit for a crystal belonging to space group $P\bar{4}3n$.

$P\bar{4}3n$, and the seed crystals are bound by the {100}, {110}, and {111} faces. Figure 1b shows a schematic diagram of the crystal morphology, indicating that only the four {111} facets and not the four $\{\bar{1}\bar{1}\bar{1}\}$ facets are expressed, which is consistent with the tetrahedral point group symmetry of the crystal structure. This immediately indicates an anisotropy in the growth rate between the ⟨111⟩ and $\langle\bar{1}\bar{1}\bar{1}\rangle$ directions.

**3.1. Growth of the {100} Facets.** Growth on the {100} facets occurs according to two different mechanisms. The first mechanism was that reported briefly previously as an interlacing spiral mechanism,[23] shown in more detail in Figure 2 (see movie m1 in the Supporting Information). This type of growth mechanism occurs when two different substeps emanate from a single screw dislocation. Each substep displays anisotropic growth but with orthogonal respective orientation. As a consequence, an interference pattern is generated, governed by the slowest growing step. In the ⟨110⟩ directions,

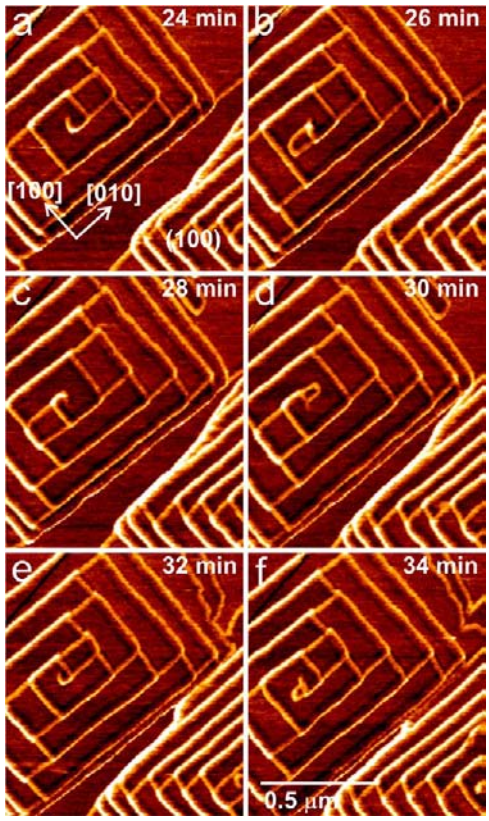


**Figure 2.** AFM lateral force micrographs showing the growth of an interlacing spiral on the (100) facet of ZnPO-SOD at (a) 24, (b) 26, (c) 28, (d) 30, (e) 32, and (f) 34 min, respectively, after the addition of a growth solution to the seed crystal.

where the growth rates are equal between the substeps, a step splitting is observed. The dislocation that generates this pair of substeps has a Burger's vector of 0.9 nm, equivalent to one unit cell in the ⟨100⟩ directions. This type of dislocation can be achieved by cleavage of bonds along the ⟨110⟩ directions, with translation of one unit cell in the ⟨100⟩ directions.

The second mechanism observed is birth-and-spread type growth, as shown by the micrographs in Figure 3. The terrace

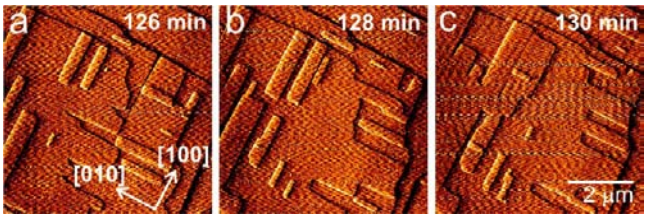


**Figure 3.** AFM deflection micrographs showing alternating anisotropic birth-and-spread growth on the (001) face of ZnPO-SOD (a) 134, (b) 136, and (c) 138 min after the addition of a growth solution to the seed crystals.

morphology is rectangular, with an alternating growth anisotropy between layers. The layers switch every half-unit-cell (terrace height measurements are 0.45 (±0.1) nm or $d_{200}$, equivalent to one-half a sodalite cage) between fast growth along [100] and slow growth along [100]. Figure 4a shows the nature of the terrace that grows on the {100} surface of ZnPO-SOD resulting from the addition of one layer of additional sodalite cages.


dx.doi.org/10.1021/ja303814p | J. Am. Chem. Soc. 2012, 134, 13066−13073

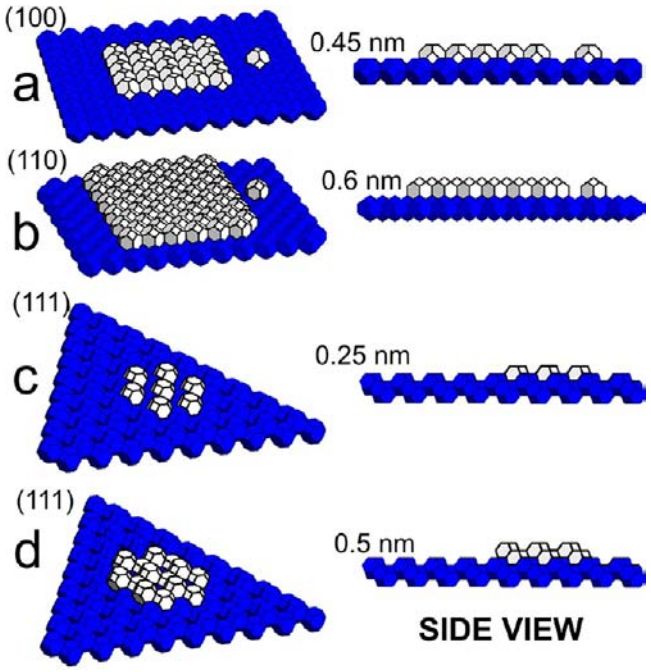


**Figure 4.** Schematic representation of possible terrace structures on the three principal facets of ZnPO-SOD. In each case, a projection is shown on the right to indicate the expected terrace height to be measured by AFM: (a) (100) surface; (b) (110) surface; (c) (111) surface showing a 0.25 nm terrace of noninterconnected sodalite cages; and (d) (111) surface showing a 0.5 nm terrace with complete through-framework interconnection.

The anisotropic growth is a consequence of crystallographic differences in the structure of ZnPO-SOD in, for instance, [100] and [010] directions, respectively, on an (001) face when the structure is considered one layer (one-half-unit-cell) at a time. The structure of ZnPO-SOD has strict alternation of zinc and phosphorus in the framework (see Figure 5a). The imbalance of charge between $PO_4^+$ and $ZnO_4^{2-}$ that leaves a residual negative charge on the framework is counter-balanced by extra-framework sodium cations. The cation balance requires three sodium cations on average per sodalite cage that are located at the four corners of a tetrahedron with one of the corners on average left vacant (see Figure 5a). This tetrahedral arrangement occupies four of the corners of a cube with the other four corners occupied by oxygen from water. The tetrahedral orientation of cations in each and every cage will be the same because the cations are located slightly displaced from a sodalite 6-ring. If the tetrahedra in adjacent cages were arranged vertex-to-vertex then the cation−cation separation across the six-ring would be too close. Consequently, the cations are highly ordered, although there is no evidence for any ordering of the 1/4 vacant sites in each sodalite cage.[42] It is important to consider whether the anisotropic growth rates are a consequence of ordering of the cations or ordering of the framework zinc and phosphorus. On the (001) surface, for example, where the anisotropic growth is between [100] and [010] directions, there is no anisotropy in the cation distribution, Figure 5a, and as a consequence cations can be discounted as the principal source of growth anisotropy. On the other hand, the framework displays a distinct difference between the [100] and [010] directions when considered as a half-unit-cell layer. Figure 5b shows two sodalite cages nucleating in these two principal directions along terrace edges. After completion of these sodalite cages of the 24 T-sites in the sodalite cage, 17 are fully condensed as $Q_4$ tetrahedra, and seven T-sites are not fully condensed as $Q_3$ tetrahedra. As a consequence, depending upon the principal direction along which the sodalite cage is nucleating, it will consist of either 4 P and 3 Zn $Q_3$ T-sites or 3 P and 4 Zn $Q_3$ T-sites. The two sodalite cages, highlighted red in Figure 5b, are therefore topologically equivalent but chemically different and hence have a different energy of stabilization (or different energy of attachment). This results in an anisotropic nucleation rate and consequent anisotropic growth rate. It should be pointed out

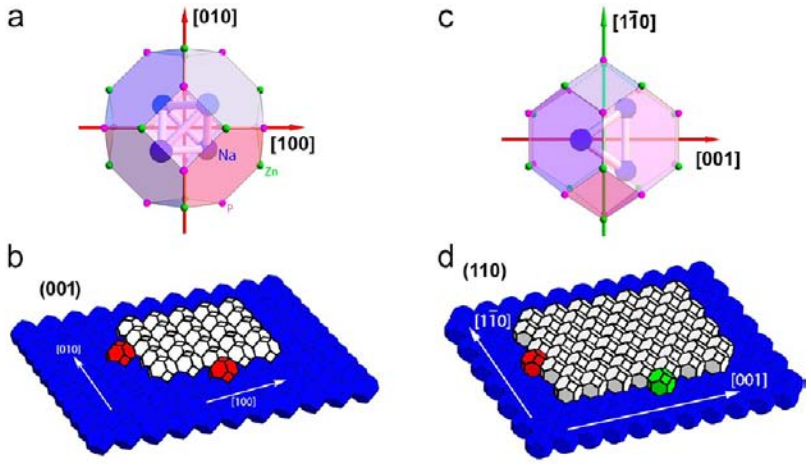


**Figure 5.** Representation of the sodalite cage ((a) viewed down [001] and (c) viewed down [110], no oxygen drawn) showing four possible cation positions for $Na^+$ (blue) arranged tetrahedrally within the cage. One site per cage is vacant with the vacancies arranged randomly. Phosphorus (pink) and zinc (green) are arranged in strict alternation in the framework. (b) Arrangement of sodalite cages for a growing terrace (white) on the (001) surface. Two nucleating sodalite cages are shown in red each with seven incomplete $Q_3$ sites; the sodalite cages are topologically identical but chemically different. These seven $Q_3$ sites are either 3 P and 4 Zn or 4 P and 3 Zn tetrahedra depending on whether the sodalite cage nucleates along [100] or [010]. (d) Schematic of the arrangement of sodalite cages for a growing terrace (white) on the (110) surface. Two nucleating sodalite cages are shown in red and green nucleating in the [1$\bar{1}$0] and [001] directions, respectively. The green sodalite cage contains seven incomplete $Q_3$ sites, and the red sodalite cage contains six incomplete $Q_3$ sites.


dx.doi.org/10.1021/ja303814p | J. Am. Chem. Soc. 2012, 134, 13066−13073

that we are not advocating that the structure grows by attachment of sodalite cages, just that closed-cage structures have substantially lower surface energy and can therefore be considered as rate-determining entities. It is the energy of such closed-cage structures that principally determines growth rates. The strong, through-framework interactions that are governing the principal growth behavior on the {100} facets are also reflected in the rectangular nature of the terraces. Straight terrace edges are maintained to mimic the energetics of the principal framework directions. In conclusion, the growth on the {100} facets of ZnPO-SOD structure is governed mainly by strong, through-framework interactions rather than via extra-framework species.

The reason that the growth anisotropy alternates between the layers is symmetry induced, as a result of an n-glide plane perpendicular to the {100} faces.[43] This results in an effective rotation of the 4-rings by 90° on the layer below, therefore switching the positions of Zn and P and the consequent number of such T-sites within a nucleation sodalite cage. This leads to a switch in the direction of the growth anisotropy for each subsequent layer, and hence the AFM observations.

**3.2. Growth of the {110} Face.** Growth of the {110} was observed ex situ to grow by a birth-and-spread mechanism and displays growth anisotropy between ⟨001⟩ and ⟨$\bar{1}$10⟩. This is shown in Figure 6a and b. Terrace height analysis gave a step

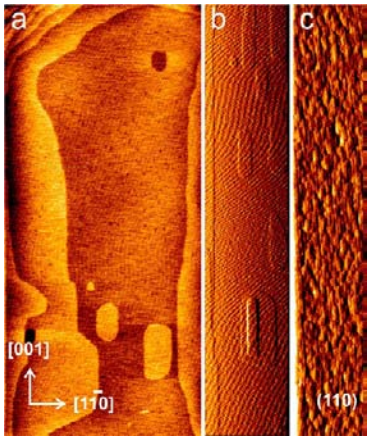


**Figure 6.** (a) Ex situ AFM height image of the (110) face of ZnPO-SOD, (b) ex situ AFM deflection image showing the terrace morphology on the (110) face, and (c) in situ AFM deflection image showing growth on the (110) face.

height of 0.6 nm, which is equivalent to capping a half completed sodalite cage to give a completed sodalite cage (see Figure 4b). In situ experiments were also performed on this face and led to a high level of nucleation on the surface as shown in Figure 6c. The rectilinear nature of the terraces on this facet again suggests that the anisotropy is a result of a strong through-framework interaction with nucleation sites at the terrace edge fundamentally different in the two principal growth directions. As can be seen in Figure 5d, nucleation of closed-cage sodalite cages on, for example, the (110) facet results in topologically distinct cages when comparing growth in the [1$\bar{1}$0] and [001] directions. The sodalite nuclei contain seven incomplete $Q_3$ sites and six incomplete $Q_3$ sites, respectively, and therefore a substantial energy of stabilization difference can be expected in the two crystallographic directions. Figure 5c shows the arrangement of extra-framework cations associated with growth on the (110) face, and this also displays an anisotropy in structure between the [1$\bar{1}$0] and [001] directions. However, this is likely to play a much smaller role in the growth anisotropy than the through-framework interactions. Unlike on the {100} facets, the growth anisotropy on the {110} facets does not switch from layer to layer consistent with the framework structure on this face.

**3.3. Growth of the {111} Face.** Growth of the {111} face of ZnPO-SOD occurs by two different mechanisms. First is a birth-and-spread mechanism as shown in Figure 7 (see movie

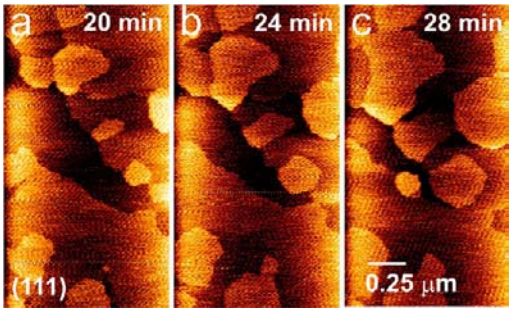


**Figure 7.** AFM height images showing birth-and-spread growth on the (111) face of ZnPO-SOD (a) 20, (b) 24, and (c) 28 min after the introduction of a growth solution.

m2 in the Supporting Information). The terrace height, measured by AFM, is 0.25 (±0.1) nm corresponding to a $d_{222}$ spacing. The second growth mechanism is a spiral growth shown in Figure 8 and also in movie m3 in the Supporting Information. This figure also reveals a combination of spiral growth and birth-and-spread growth occurring simultaneously. The terrace height for the spiral growth is 0.5 (±0.1) nm corresponding to a $d_{111}$ spacing.

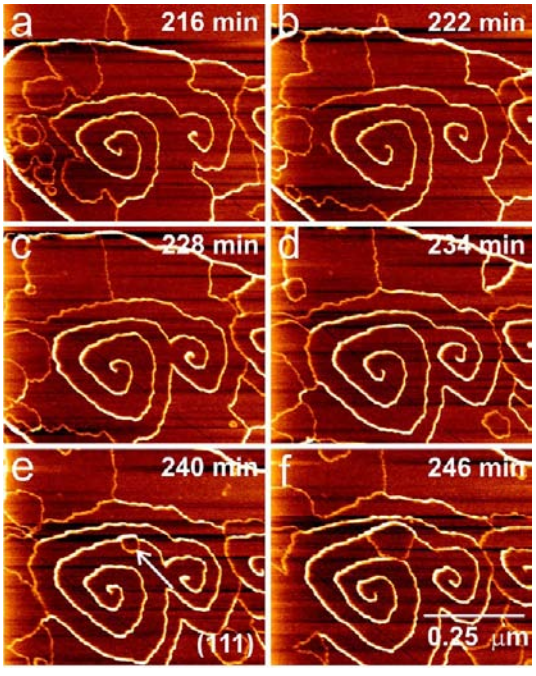


**Figure 8.** AFM lateral force micrographs showing spiral and birth-and-spread growth on the (111) face (a) 214, (b) 222, (c) 230, and (d) 238 min after the addition of a growth solution.


dx.doi.org/10.1021/ja303814p | J. Am. Chem. Soc. 2012, 134, 13066−13073

Considering first the birth-and-spread growth, a marked difference from growth observed on both {100} and {110} facets is that the terraces show isotropic growth with ill-defined terrace edges. The terrace height of 0.25 nm is equivalent to the addition of a single layer of 6-rings onto the surface of a {111} face (see Figures 4c and 9). These six-rings have no direct

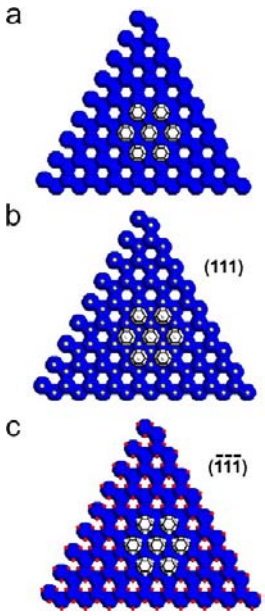


**Figure 9.** Schematic representation of a 0.25 nm terrace (white) growing on the (111) and $(\bar{1}\bar{1}\bar{1})$ surface of ZnPO-SOD structure. The through-framework interconnectivity of such a terrace is interrupted (a), and the cation distribution (shown in yellow and red) is different on (b) (111) versus (c) $(\bar{1}\bar{1}\bar{1})$.

through-framework connectivity, and consequently the continuous terrace structure is connected through the extra-framework cations and zeolitic (bound) water. In the aluminosilicate, the extra-framework species were found to interact relatively strongly, both with each other and with the framework. This led to the formation of water/cation clusters, with the water hydrogen bonded to the framework. This therefore would lead to relatively strong interactions between framework and extra-framework species. The structure of the zincophosphate analogue seems to agree with this model, as the positions given in the initial Rietveld refinement suggest.[39] Despite these extra-framework interactions being relatively strong, they will be much weaker than the through-framework interconnections, and this relative weakness of interconnectivity is reflected in the ill-defined shape of the terraces. More importantly, this is the first experimental measurement of the relative importance of the extra-framework material during the growth of a nanoporous framework oxide material. It illustrates quite clearly that zeolites should not be considered as nanoporous in terms of crystal growth but as dense phase structures exhibiting a range of strengths of interconnectivity, strong through-bond linkages and weaker through-extra-framework-species linkages. The effect of the extra-framework species is further manifested in the overall crystal habit. Growth on the {111} and $\{\bar{1}\bar{1}\bar{1}\}$ facets is exactly equivalent considering only the framework interconnectivity, even considering the strict zinc/phosphorus ordering. However, the decoration of the {111} and $\{\bar{1}\bar{1}\bar{1}\}$ growth surfaces with cations is markedly different, because of the cation ordering, resulting in a very different polarity of the two surfaces (see Figure 9). The growth rates on the two correspond facets are so different that only one of the two facets is expressed, resulting in the morphology with tetrahedral point group symmetry shown in Figure 1.

The spiral growth terraces observed on {111} are twice the height of the birth-and-spread growth terraces, resulting in the terrace structure shown in Figure 4d. The terrace now has through-framework interconnectivity, and this is reflected in the more angular terrace morphology with near 3-fold symmetry. This is more consistent with that seen on the {100} and {110} facets. Although we are unable to verify the structure of the screw dislocation at this time, it is consistent with a structure identical to the screw dislocation emanating on the {100} facet with a dislocation vector parallel to ⟨100⟩. Such a dislocation would result in no loss of framework interconnectivity and a preservation of the strict zinc/phosphorus alternation. It is also interesting that birth-and-spread growth is nucleated at the spiral terrace edges (indicated in Figure 8e), suggesting that either there is a localized higher level of supersaturation along the terrace edge or that the structural modification at the edge lowers the surface energy and promotes nucleation.

**3.4. Defect Growth.** The AFM studies on ZnPO-SOD structure also reveal a number of growth processes initiated by either intrinsic or extrinsic defects other than spiral growth at a screw dislocation.

*3.4.1. Zn/P Order Switching on the {100} Surface.* During both growth and dissolution of ZnPO-SOD, the occurrence of another type of defect is commonplace. This type of defect is shown in Figure 10 and manifests itself in lateral force microscopy as a bright line parallel to the ⟨110⟩ direction (see movies m4, m5, and m6 in the Supporting Information). Lateral force is measured as a twisting of the cantilever. On either side of this feature, the growth anisotropy of terraces is observed to switch (highlighted by white arrows in Figure 10d). Further, the step-splitting characteristic of the interlacing spiral pattern disappears across this defect. This suggests that across the line there is a switch in the Zn:P ordering. This is shown in Figure 10b. In this structural diagram, the change in Zn:P ordering is highlighted across the white line that passes across the ⟨110⟩ direction, representing the defect. The defect is also the source of multiple spiral centers. In the cross-section in Figure 10c, the point at which the dislocation occurs is highlighted and, within the error of the experiment, shows no height difference. The dislocation proposed results in complete connectivity at the source of the dislocation, with only a change in the Zn/P ordering across the defect.

*3.4.2. Mound Growth.* Observations of the {100} face of ZnPO-SOD reveal the formation of square-based growth mounds aligned with the base parallel to the crystal edges, such as those shown in Figure S1 in the Supporting Information. Growth mounds of this type, initiated by enhanced surface nucleation at a specific site, have previously been observed for other open framework materials. For zeolite A, the first observations of these mounds were made by Sugiyama et al., who found square-based pyramidal mounds forming on the {100} face parallel to the edges of the crystals; however, no explanation for their origin was initially forwarded.[44] Dumrul et al. also observed these mounds, and found that, in many cases, they were formed with a growth protrusion or crystallographic fault at their apex. It was postulated that the mounds were formed due to a lower activation energy for surface nucleation, caused by small particles acting as the equilibrium shaped nuclei, or by forming


dx.doi.org/10.1021/ja303814p | J. Am. Chem. Soc. 2012, 134, 13066−13073

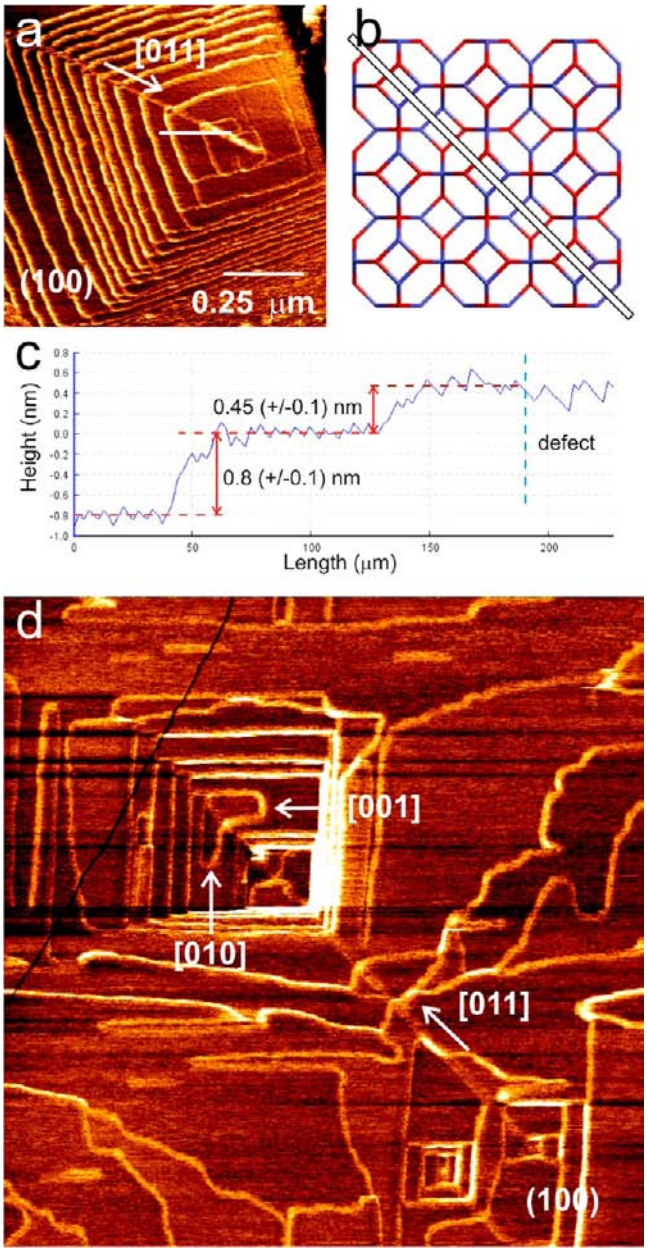


**Figure 10.** (a) LFM micrograph showing low-angle defect during growth, (b) structural diagram showing the change in Zn/P ordering across the defect (white line), (c) representative cross-section of the area shown in Figure 9a, and (d) LFM micrograph showing the same type of defect observed during dissolution.

faulted two-dimensional embryos, becoming critical twin nuclei and therefore generating new terraces by a twin-plane re-entrant corner mechanism.[45] In addition to this, Meza et al. also observed protrusions at the apex of pyramids on the surface of zeolite A crystals, attributed either to foreign particles or as the result of an existing dislocation. It was shown to be possible to dissolve these protrusions, leading to voids at the apex of the pyramids.[11]

Figure S2 in the Supporting Information shows a time sequence of AFM images of the growth of ZnPO-SOD {100} layers that eventually result in a growth mound (see movie m7 in the Supporting Information). Initially during this experiment, growth proceeded via a birth-and-spread mechanism similar to that shown in Figure 3. However, after a certain time, growth mounds began forming over various parts of the crystal face. Each layer nucleates at the same position on the crystal surface, and there is no indication of any foreign material at the surface. The growth is also not tip induced as growth mounds appear all over the crystal face in regions not scanned by the AFM. This, therefore, represents an intrinsic growth with enhanced surface nucleation at a specific point on the crystal surface. Our measurements have not been able to reveal any surface structural difference at the point of surface nucleation. However, a clue to the possible presence of line defects that extend to the {100} surface of ZnPO-SOD is shown in the lateral deflection images in Figure S3 of the Supporting Information. During these measurements, taken on the same crystal, some unusual observations were made that could be related to the initiation of this mound growth. Lateral deflection measures the twisting of the cantilever as it moves across the sample and is related to the friction of a sample, because samples with higher friction will cause a larger twist of the cantilever. In the micrographs presented, a larger twist of the cantilever is shown as a brighter feature on the micrograph. During the experiment, several "bright spots" were present on the surface of the crystal, a cluster of which is highlighted throughout Figure S3 in the Supporting Information. These bright spots can be tracked through multiple scans and do not disappear after multiple terraces grow over them. These bright spots have no height, and therefore suggest the presence of defects at the surface. Similar defects could be the surface nucleation sites for mound growth; however, at the present time, we have not been able to directly correlate these two phenomena.

*3.4.3. Extended Defect.* Figure S4 in the Supporting Information shows an extended defect on the {100} surface that traverses an entire crystal in the ⟨100⟩ direction. The defect manifests as a very low angle grain boundary at the surface of the crystal that suggests surface strain possibly as the result of some internal macroscopic defect that the crystal is trying to accommodate. The result at the surface of the crystal is that along the line of the defect multiple screw dislocations are formed. A similar observation has been observed previously on the topologically identical metal organic framework crystal ZIF-8, which also has the SOD structure.[46]

*3.4.4. Extrinsic Defects.* Figure S5 in the Supporting Information shows an example of the formation of growth mounds in the presence of extraneous foreign material similar to those observed in zeolite A. It is unclear in this case the nature of the foreign particles on the surface, and whether or not they are ordered. In Figure S5 in the Supporting Information, many of these particles can be clearly seen on the crystal surface. When growing in situ, these particles act as a site that promotes nucleation, as evidenced in the sequence shown in Figure S5 (and see movie m8 in the Supporting Information). In this sequence, the supersaturation of the growth solution was low, meaning that surface nucleation on an open terrace was not observed. However, it can be seen that many layers formed quickly on top of the particle, showing an enhanced nucleation rate. For a few layers, the enhanced nucleation effected by the particle continued; however, after ca. 8 layers, the particle no longer seemed to have an effect on growth. At this point, 2-D nucleation ceased and the terrace spread out, leaving a large flat area at the peak of the growth mound. A similar type of assisted nucleation has also been observed to be induced through intergrowth formation (see Figure S6 in the Supporting Information). From this image, it


dx.doi.org/10.1021/ja303814p | J. Am. Chem. Soc. 2012, 134, 13066−13073

can be seen that throughout the sample there was a lot of intergrowth between sodalite crystals, leaving distorted morphologies and protrusions from the surfaces (highlighted by arrows). As can be seen, the interface between the intergrowth became preferential site at which nucleation occurred, allowing the growth of two mounds, each one centered on one of these features, which developed throughout the experiment performed. These mounds eventually dominated the whole {100} surface, allowing the continuation of growth of this face at supersaturations where 2-D nucleation was not observed.

**3.5. Anisotropic Friction.** Lateral force microscopy is a useful tool for studying surface friction.[47] Curiously, ZnPO-SOD displays marked anisotropic friction on the (001) facet between the [100] and [010] directions (see Figure 11). This

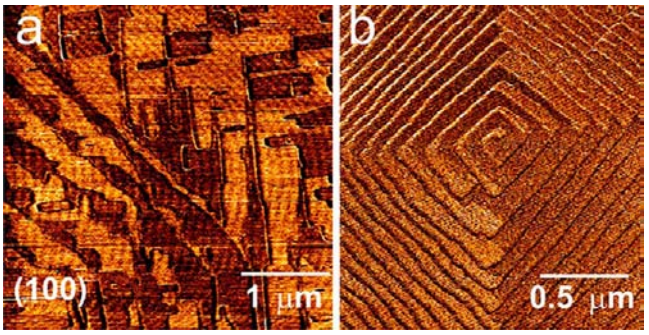


**Figure 11.** AFM lateral force micrographs showing anisotropic friction during (a) birth-and-spread and (b) spiral growth on the {100} face of ZnPO-SOD.

effect is observed for both birth-and-spread and spiral type growth. The lighter areas on the terraces show areas of higher friction, and the darker areas indicate lower friction. Each terrace displays the opposite anisotropy to the terrace above or below, and this observation can be related to the crystallography of the surface. The anisotropy follows the same pattern as the anisotropy of the terrace growth rates. By rotating the sample by 90°, it was possible to reverse the contrast, which proved that it is related to the direction the tip moved across the terrace. Friction anisotropy has been observed in other systems, where it has been related to the orientation of certain structural groups to the scan direction.[48−50] In this case, the anisotropy on this facet of the crystal results only from the zinc/phosphorus ordering and not from the extra-framework cations. The crystal surface will be terminated either with terminal −OH groups or ordered water molecules. The suggestion from this work is, therefore, that the organization of such groups displays at most 2-fold symmetry as a consequence of the zinc/phosphorus ordering. To our knowledge, there are no experimental crystallographic data to confirm such an assertion, and the only route to test such a hypothesis is through molecular modeling. This discovery of anisotropic friction at the surface of a framework material is, perhaps, a first step in the complicated task to analyze the molecular details of surface structure in a framework material.

**3.6. Lateral Force Highlights Growth Processes.** In a previous study of the dissolution of zeolite L,[21] it was observed that, when operating the AFM to monitor lateral deflection, there was a substantial deflection registered specifically at the point of the surface that was dissolving. In this work, the same phenomenon is apparent during crystal growth. The effect can be seen in Figures 2, 8, 10, and S2 in the Supporting Information as a bright white feature around the terrace edges. This large lateral deflection, which is observed whether the tip is mounting or dis-mounting a terrace edge, is caused by the crystal growth process imparting an energy into the tip. The amount of energy imparted is directly proportional to the degree of reaction occurring at the terrace edge as a terrace with a double step height imparts twice the energy at a terrace edge with a single step height.

This energy imparted can be calculated by first converting the output lateral deflection voltage into a force. To perform this operation, the trace and retrace images over the same area are taken. This is shown in Figure S7 in the Supporting Information. The extra friction created by traversing the step is then calculated as the difference between the baseline (short arrow) and the peak (long arrow), divided by 2 to give voltage difference per scan. This voltage can be converted into a force using the following:[51]

$$F_L = 3/2K_L(h/l)S_L V_L \quad (1)$$

where $F_L$ is the lateral force, $K_L$ is the lateral spring constant, $h$ and $l$ represent the height and length of the cantilever used, $S_L$ is the lateral sensitivity, and $V_L$ is the lateral voltage. The force measured can then be converted to an energy using:[21]

$$E_L = {F_L}^2/2K_L \quad (2)$$

where $E_L$ is the energy of the lateral force. Combining the two, it can be seen that $E_L \propto {V_L}^2$. Therefore, comparing lateral force measurements from a single image can give information on the energy differences involved. These measurements show that on the {100} face the energy imparted traversing the terraces of double height is 2.1 (±0.2) times the energy when a monolayer is traversed.

By understanding the mechanics of the tip, it should be possible to determine the absolute energy imparted to the tip as a result of these processes, and this is currently under investigation. In principle, however, lateral force is a very sensitive tool to highlight the nanoscopic regions of a crystal surfaces where reactions are occurring and ultimately should be able to discriminate between processes with different enthalpies of reaction.

## 4. CONCLUSIONS

This work has revealed the nanoscopic details of the growth mechanism on a nanoporous zincphosphate with sodalite structure by monitoring growth in situ by AFM. A distinction can be made between growth facilitated via strong framework interconnectivity from that facilitated via weaker extra-framework cations and hydrogen-bonded water. The overall crystal growth must be viewed as that of a dense-phase material rather than that of an open-pore material as all of the elements of the structure, both framework and extra-framework, play an important part in the process. This type of picture of crystal growth is likely to be universal for nanoporous materials, whether inorganic, inorganic/organic, or purely organic. Sodalite serves as a very good model system for the study of crystal growth mechanisms due to the simplicity of the structure and ordering of metal atoms within the framework. Subtle differences in growth kinetics as a result of the stabilization of zinc versus phosphorus in the framework can be observed, and the lessons learned will have important ramifications for related ordered aluminosilicate zeolite phases.

This work also identifies for the first time a number of growth defects in the sodalite system as well as the first report of friction anisotropy in a framework material.

## ■ ASSOCIATED CONTENT

### Supporting Information

Figures and movie descriptions. Movies of AFM growth sequences available in QuickTime format. This material is available free of charge via the Internet at http://pubs.acs.org.

## ■ AUTHOR INFORMATION


### Corresponding Author

m.anderson@manchester.ac.uk


### Notes

The authors declare no competing financial interest.

## ■ ACKNOWLEDGMENTS

We wish to thank EPSRC, Leverhulme Foundation, and ExxonMobil Research and Engineering for financial support of this project.

## ■ REFERENCES


(1) Anderson, M. W.; Agger, J. R.; Thornton, J. T.; Forsyth, N. *Angew. Chem., Int. Ed. Engl.* **1996**, *35*, 1210−1213.

(2) Agger, J. R.; Pervaiz, N.; Cheetham, A. K.; Anderson, M. W. *J. Am. Chem. Soc.* **1998**, *120*, 10754−10759.

(3) Agger, J. R.; Hanif, N.; Anderson, M. W. *Angew. Chem., Int. Ed.* **2001**, *40*, 4065.

(4) Agger, J. R.; Hanif, N.; Cundy, C. S.; Wade, A. P.; Dennison, S.; Rawlinson, P. A.; Anderson, M. W. *J. Am. Chem. Soc.* **2003**, *125*, 830−839.

(5) Meza, L. I.; Agger, J. R.; Logar, N. Z.; Kaucic, V.; Anderson, M. W. *Chem. Commun.* **2003**, 2300−2301.

(6) Meza, L. I.; Anderson, M. W.; Agger, J. R. *Chem. Commun.* **2007**, 2473−2475.

(7) Meza, L. I.; Anderson, M. W.; Agger, J. R.; Cundy, C. S.; Chong, C. B.; Plaisted, R. J. *J. Am. Chem. Soc.* **2007**, *129*, 15192−15201.

(8) Shoaee, M.; Agger, J. R.; Anderson, M. W.; Attfield, M. P. *CrystEngComm* **2008**, *10*, 646−648.

(9) Stevens, S. M.; Cubillas, P.; Jansson, K.; Terasaki, O.; Anderson, M. W.; Wright, P. A.; Castro, M. *Chem. Commun.* **2008**, 3894−3896.

(10) Brent, R.; Anderson, M. W. *Angew. Chem., Int. Ed.* **2008**, *47*, 5327−5330.

(11) Meza, L. I.; Anderson, M. W.; Slater, B.; Agger, J. R. *Phys. Chem. Chem. Phys.* **2008**, *10*, 5066−5076.

(12) Stevens, S. M.; Jansson, K.; John, N. S.; Terasaki, O.; Anderson, M. W.; Castro, M.; Wright, P. A.; Cubillas, P. *Zeolites and Related Materials: Trends, Targets and Challenges, Proceedings of the 4th International Feza Conference*; 2008; Vol. *174*, pp 775−780.

(13) Shoaee, M.; Anderson, M. W.; Attfield, M. R. *Angew. Chem., Int. Ed.* **2008**, *47*, 8525−8528.

(14) John, N. S.; Scherb, C.; Shoaee, M.; Anderson, M. W.; Attfield, M. P.; Bein, T. *Chem. Commun.* **2009**, 6294−6296.

(15) Stevens, S. M.; Jansson, K.; Xiao, C.; Asahina, S.; Klingstedt, M.; Gruner, D.; Sakamoto, Y.; Miyasaka, K.; Cubillas, P.; Brent, R.; Han, L.; Che, S.; Ryoo, R.; Zhao, D.; Anderson, M. W.; Schuth, F.; Terasaki, O. *JEOL News* **2009**, *44*, 15.

(16) Stevens, S. M.; Cubillas, P.; Jansson, K.; Terasaki, O.; Anderson, M. W. *J. Phys. Chem. C* **2009**, *113*, 18441−18443.

(17) Cubillas, P.; Castro, M.; Jelfs, K. E.; Lobo, A. J. W.; Slater, B.; Lewis, D. W.; Wright, P. A.; Stevens, S. M.; Anderson, M. W. *Cryst. Growth Des.* **2009**, *9*, 4041−4050.

(18) John, N. S.; Stevens, S. M.; Terasaki, O.; Anderson, M. W. *Chem.-Eur. J.* **2010**, *16*, 2220−2230.

(19) Brent, R.; Stevens, S. M.; Terasaki, O.; Anderson, M. W. *Cryst. Growth Des.* **2010**, *10*, 5182−5186.

(20) Brent, R.; Lobo, A. J. W.; Lewis, D. W.; Anderson, M. W. *J. Phys. Chem. C* **2010**, *114*, 18240−18246.

(21) Brent, R.; Cubillas, P.; Stevens, S. M.; Jelfs, K. E.; Umemura, A.; Gebbie, J. T.; Slater, B.; Terasaki, O.; Holden, M. A.; Anderson, M. W. *J. Am. Chem. Soc.* **2010**, *132*, 13858−13868.

(22) Holme, B.; Cubillas, P.; Cavka, J. H.; Slater, B.; Anderson, M. W.; Akporiaye, D. *Cryst. Growth Des.* **2010**, *10*, 2824−2828.

(23) Holden, M. A.; Cubillas, P.; Anderson, M. W. *Chem. Commun.* **2010**, *46*, 1047−1049.

(24) Cubillas, P.; Holden, M. A.; Anderson, M. W. *Cryst. Growth Des.* **2011**, *11*, 3163−3171.

(25) Anderson, M. W.; Agger, J. R.; Meza, L. I.; Chong, C. B.; Cundy, C. S. *Faraday Discuss.* **2007**, *136*, 143−156.

(26) Cubillas, P.; Anderson, M. W. In *Zeolites and Catalysis: Synthesis, Reactions and Applications*; Cejka, J., Corma, A., Zones, S., Eds.; Wiley-VCH Verlag GmbH & Co. KGaA: New York, 2010; pp 1−55.

(27) Pauling, L. *Z. Kristallogr.* **1930**, *74*, 213−225.

(28) Johnson, G. M.; Mead, P. J.; Weller, M. T. *Microporous Mesoporous Mater.* **2000**, *38*, 445−460.

(29) Gier, T. E.; Stucky, G. D. *Nature* **1991**, *349*, 508−510.

(30) Bu, X. H.; Feng, P. Y.; Gier, T. E.; Zhao, D. Y.; Stucky, G. D. *J. Am. Chem. Soc.* **1998**, *120*, 13389−13397.

(31) Vaughan, D. E. W.; Strohmaier, K. G.; Pickering, I. J.; George, G. N. *Solid State Ionics* **1992**, *53*−*56*, 1282−1291.

(32) van den Berg, A. W. C.; Bromley, S. T.; Jansen, J. C. *Microporous Mesoporous Mater.* **2005**, *78*, 63−71.

(33) Barrer, R. M.; Vaughan, D. E. W. *J. Phys. Chem. Solids* **1971**, *32*, 731−&.

(34) Thijs, A.; Vansant, E. F. *J. Inclusion Phenom.* **1987**, *5*, 289−296.

(35) Williams, E. F.; Hodgson, W. G.; Brinen, J. S. *J. Am. Ceram. Soc.* **1969**, *52*, 139−&.

(36) Khajavi, S.; Kapteijn, F.; Jansen, J. C. *J. Membr. Sci.* **2007**, *299*, 63−72.

(37) Khajavi, S.; Sartipi, S.; Gascon, J.; Jansen, J. C.; Kapteijn, F. *Microporous Mesoporous Mater.* **2010**, *132*, 510−517.

(38) Baerlocher, C.; McCusker, L. B.; Olson, D. H. *Atlas of Zeolite Framework Types*, 6th ed.; Elsevier: New York, 2007.

(39) Nenoff, T. M.; Harrison, W. T. A.; Gier, T. E.; Stucky, G. D. *J. Am. Chem. Soc.* **1991**, *113*, 378−379.

(40) Rajic, N.; Logar, N. Z.; Kaucic, V. *Zeolites* **1995**, *15*, 672−678.

(41) Harrison, W. T. A.; Gier, T. E.; Stucky, G. D.; Broach, R. W.; Bedard, R. A. *Chem. Mater.* **1996**, *8*, 145−151.

(42) Felsche, J.; Luger, S.; Baerlocher, C. *Zeolites* **1986**, *6*, 367−372.

(43) van Enckevort, W. J. P.; Bennema, P. *Acta Crystallogr., Sect. A* **2004**, *60*, 532−541.

(44) Sugiyama, S.; Yamamoto, S.; Matsuoka, O.; Nozoye, H.; Yu, J.; Zhu, G.; Qiu, S.; Terasaki, I. *Microporous Mesoporous Mater.* **1999**, *28*, 1−7.

(45) Dumrul, S.; Bazzana, S.; Warzywoda, J.; Biederman, R. R.; Sacco, A. *Microporous Mesoporous Mater.* **2002**, *54*, 79−88.

(46) Moh, P. Y. Ph.D. Thesis, University of Manchester, 2012.

(47) Cubillas, P.; Higgins, S. R. *Geochem. Trans.* **2009**, *10*, 7.

(48) Bluhm, H.; Schwarz, U. D.; Meyer, K. P.; Wiesendanger, R. *Appl. Phys. A: Mater. Sci. Process.* **1995**, *61*, 525−533.

(49) Overney, R. M.; Takano, H.; Fujihira, M.; Paulus, W.; Ringsdorf, H. *Phys. Rev. Lett.* **1994**, *72*, 3546−3549.

(50) Shindo, H.; Shitagami, K.; Sugai, T.; Kondo, S. *Phys. Chem. Chem. Phys.* **1999**, *1*, 1597−1600.

(51) Gnecco, E.; Bennewitz, O. P.; Socoliuc, A.; Meyer, E. In *Nanotribology and Nanomechanics*; Bhushan, B., Ed.; Springer: Berlin, Heidelberg, New York, 2005; pp 483−533.